ELSEVIER

Journal of Atmospheric and Solar-Terrestrial Physics 66 (2004) 927–932

Journal of ATMOSPHERIC AND SOLAR-TERRESTRIAL PHYSICS

www.elsevier.com/locate/jastp

Analogue model, relating K_p index to solar wind parameters

Borislav Andonov, Plamen Muhtarov, Ivan Kutiev*

Geophysical Institute, Bulgarian Academy of Sciences, Acad. G. Bonchev str., bl. 3, Sofia 1113, Bulgaria

Received 20 November 2002; received in revised form 18 February 2004; accepted 25 March 2004

Abstract

In a previous work the authors have developed a model, providing K_p as a function of the interplanetary magnetic field B_z component. They introduced a modified B_z function (denoted as B_{zm}), exhibiting a delayed reaction to B_z changes. The modified function B_{zm} was defined by using the analogy with a damping RC-circuit output voltage. The delaying reaction of B_{zm} to B_z was characterized by two time constants, one for rising and one for decreasing parts of B_z. The cross-correlation between K_p and B_{zm} has increased to 0.7, compared with -0.4 between K_p and B_z. In this paper, new dependences of K_p on solar wind velocity and dynamic pressure are included in the model to improve its accuracy. These solar wind parameters are found to correlate best with K_p. The hourly interpolated values are also added to the 3-h K_p values to increase the statistics. The new K_p data set is denoted as K_{p1}. The mean dependence of K_p on B_{zm} and dynamic pressure are approximated with parabolas, while the dependence on the velocity is linear. The constants in the model expression are obtained by using ACE data (1998–2000). The overall model error is estimated at 0.63 units K_p. The improvement over the previous simpler dependence in terms of the model error is about 30%.

Keywords: Solar wind parameters; K_p index; Geomagnetic activity; Analogue model; Delayed function of B_z

1. Introduction

The planetary indices of geomagnetic activity reflect the complex non-linear transfer of energy deposited by solar wind into magnetosphere with a subsequent interaction with polar ionosphere. To avoid complexity of the physical processes in modelling this transfer, many investigators use empirical relations between solar wind and geomagnetic activity parameters, which are based on some well-known physical analogues. Hones (1979) and Klimas et al. (1992) have used the dripping-faucet analogue to describe the plasmoid formation in the magnetosphere tail, the main transposer of solar wind energy into substorm activity. Baker et al. (1990) and Vassilliadis et al. (1993) have used an electric LRC circuit as a damped linear oscillator to represent the return of a "perturbed" magnetosphere to its "quiet" state.

Muhtarov and Andonov (2000), further denoted as MA, developed a model relating K_p to the interplanetary magnetic field (IMF) B_z component by using an electric diode rectifier circuit (DRC) analogue. The circuit they used is similar to that of Vassilliadis et al. (1993), in which the inductance part was replaced with a half-wave diode rectifier. MA used B_z as an input voltage, while the output voltage they defined as a "modified" B_z (B_{zm}) having positive variations only. The hourly values of the new quantity B_{zm} were correlated with the hourly interpolated K_p values to obtain the model parameters. Using 27 years of IMF data (1973–1999), MA estimated that B_{zm} improved the correlation between B_z and K_p from -0.4 to 0.7. In this paper, we use the same approach as in MA, adding dependences on solar wind dynamic pressure and velocity. For this purpose, we use a database containing ACE data collected between 1998 and 2000.

2. The DRC circuit model

It is well accepted that B_z is a main driver of geomagnetic activity and of K_p variations, in particular (see Kamide

* Corresponding author. Fax: +359-2-971-3005.
E-mail address: kutievi@geophys.bas.bg (I. Kutiev).

1364-6826/$ - see front matter
doi:10.1016/j.jastp.2004.03.006

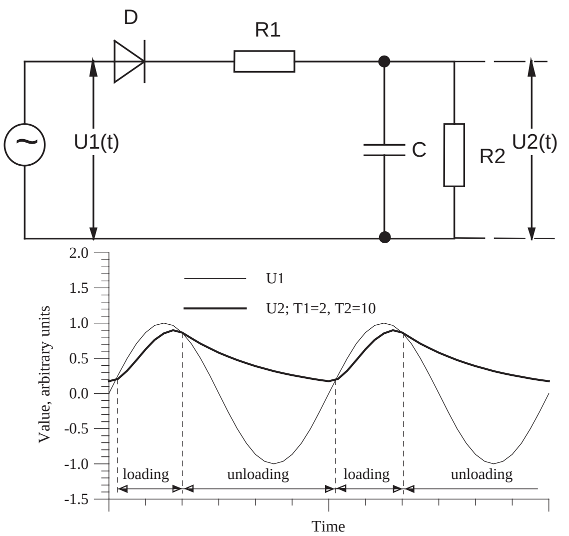

Fig. 1. (a) Equivalent electric circuit DRC, giving the delayed reaction of the output voltage U_2 to the input voltage U_1. D is a half-wave diode rectifier, C is a capacitor, R_1 and R_2 are resistors; (b) a sample of a sinusoidal input voltage U_1 and the resulting output voltage U_2. Loading and unloading phases are marked with horizontal bars. T_1 and T_2 are assured arbitrary to demonstrate the functioning of the circuit and do not relate to the values considered in the paper.

et al., 1998 and references therein). The negative turning of B_z causes an increase of K_p, known as "driven" response (Klimas et al., 1991). The increase of B_z or turning positive is not followed by an immediate and proportional decrease of K_p. The changes of K_p appear more gradual and delayed. MA found that the cross-correlation between B_z and K_p had a maximum at a time lag of about 2 h. This means that K_p best correlates with B_z from the previous 2 h. In order to improve the dependence of K_p on B_z, MA introduced a new function of B_z (denoted as B_{zm}), which is positive and contains a delayed reaction to B_z changes. To do this, they used an analogy with another inertial system, which involves loading and unloading processes with different time constants. An electrical circuit shown on Fig. 1a can represent such a system. The circuit includes a half-wave diode rectifier D, a smoothing capacitor C and two resistors R_1 and R_2. MA considered that the input voltage U_1 was a step-like function, formed by discrete values at arbitrary moments of time. If $R_2 \gg R_1$, the output voltage U_2 within the time-step $[t_i, t_{i+1}]$ is given by a well-known relationship:

$$U_2(t_{[i+1]}) = \begin{cases} (U_2(t_i) - U_1(t_i))\exp\left(-\dfrac{t_{[i+1]} - t_i}{T_1}\right) + U_1(t_i); \\ \quad U_2(t_i) < U_1(t_i) \\ U_2(t_i)\exp\left(-\dfrac{t_{[i+1]} - t_i}{T_2}\right); \\ \quad U_2(t_i) > U_1(t_i), \end{cases} \tag{1}$$

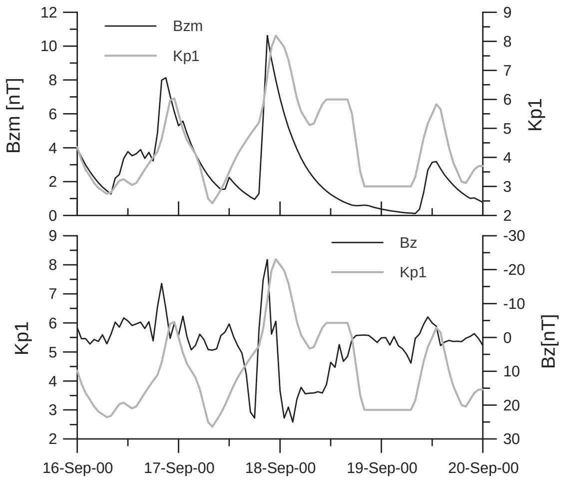

Fig. 2. B_z, B_{zm} and K_{p1} variations during 16–19 September 2000. Upper panel: B_{zm} and K_{p1} (scale on the right); lower panel: K_{p1} and B_z (scale on the right).

where $T_1 = R_1C$ and $T_2 = R_2C$. Expressions (1) have recurrent feedback: the voltage U_2 obtained from the previous step $[t_{i-1}, t_i]$ is placed on the right-hand side of the equations for obtaining U_2 in the next step $[t_i, t_{i+1}]$. The first expression in (1) represents a process of loading the capacitor C with a time constant T_1, while the second expression represents the unloading process with a time constant T_2. The loading takes place while U_1 is higher than U_2 and the diode is open. If U_1 becomes lower than U_2, the diode is closed and the capacitor starts discharging through the resistor R_2. The whole process is schematically presented on Fig. 1b. The input voltage U_1 is represented as a simple sinusoid (thin line) and the output voltage U_2 is given by the solid line. The loading takes place when $U_1 > U_2$. The output voltage U_2 accepts now only positive values, gradually decreasing when U_1 is lower. The time constants T_1 and T_2 shown in Fig. 1b are arbitrary, just to demonstrate the functioning of the circuit, and do not relate to the values considered later in the paper. Making use of the analogy with this electrical scheme, MA defined B_{zm} through Eq. (1) with a replacement of U_1 with $-B_z$ and $U_2$with B_{zm}.

As MA, here we also add the hourly K_p values, obtained by a linear interpolation between the observed 3-h K_p index, to the K_p data set. The only reason for that is to increase statistics, while we use the hourly values of the solar wind parameters B_z, velocity and dynamic pressure. In order to distinguish between the new data set and the observed 3-h K_p index, we denote hereafter the new data set as "K_{p1}". Fig. 2 shows a sample of B_z, B_{zm} and K_{p1} variations during the period 16–19 September 2000. B_{zm} is calculated by using Eq. (1), setting $T_1 = 0.8$ and $T_2 = 9$ h, as obtained by MA. MA has obtained these values through a procedure explained below, using IMF data. B_z and K_{p1} variations are compared in the lower panel, while B_{zm} and K_{p1} variations

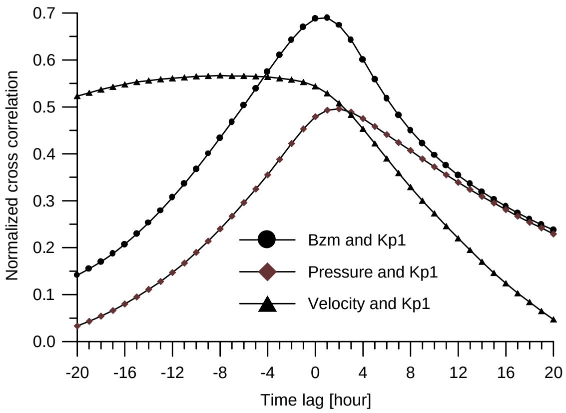

Fig. 3. Normalized cross-correlation of K_{p1} with B_{zm} (dots), solar wind dynamic pressure (diamonds) and velocity triangles.

are shown in the upper panel. B_z scale is reversed, with negative B_z upward. Two spikes of negative B_z occur on 16 and 17 September, followed by a delayed decrease of B_{zm}. B_{zm} changes resemble those of K_{p1}. In this particular sample, B_{zm} increase faster than K_{p1}, which means that T_1 is assured smaller than needed. In the unloading phase, B_{zm} decrease matches better than K_{p1} changes. It is worth noting, that MA has determined T_1 and T_2 by using 27 years of data, but obviously these average time constants do not assure the best agreement between K_{p1} and B_{zm} in any individual case.

Using ACE solar wind data, we calculated the cross-correlation between K_{p1} and the hourly values of B_{zm}, solar wind velocity V and dynamic pressure P ($P = 1.673 \times 10^{-6}\ nV^2$, n is the ion density). Here B_{zm} is in nanotesla, P in nanopascal, n in cm^{-3} and V in km/s. The cross-correlation functions are shown in Fig. 3 as functions of the time lag in the range $(-20, 20)$ h. B_{zm} (calculated with $T_1 = 3$ and $T_2 = 7$ h, as will be shown later) has the highest correlation with K_{p1}, reaching 0.7 at the time lag of 1 h. The correlation of K_{p1} with solar wind dynamic pressure has a peak of 0.5 at the time lag of 2 h, while the correlation with solar wind velocity has a broad maximum of 0.57 in the negative time lags. The cross-correlation of K_{p1} with solar wind density has a maximum value of 0.25 at the time lag of 3 h and is practically insignificant. Fig. 3 shows the cross-correlation at both positive and negative time lags because formally this function is not symmetric. Positive time lags indicate forecasting capabilities, while the negative time lags do not. For these particular dependences, however, when we consider a cause–effect relationship between solar wind parameters and K_{p1}, negative time lags are meaningless. The high cross-correlation between velocity V and K_{p1} at negative time lags possibly is due to the different time scale variations of the velocity and K_{p1}. Data show that over the large time scale, e.g. days, both quantities correlate fairly well, but for the time scale of hours correlation is poor. In this latter case K_{p1} spikes are observed to precede those of V,

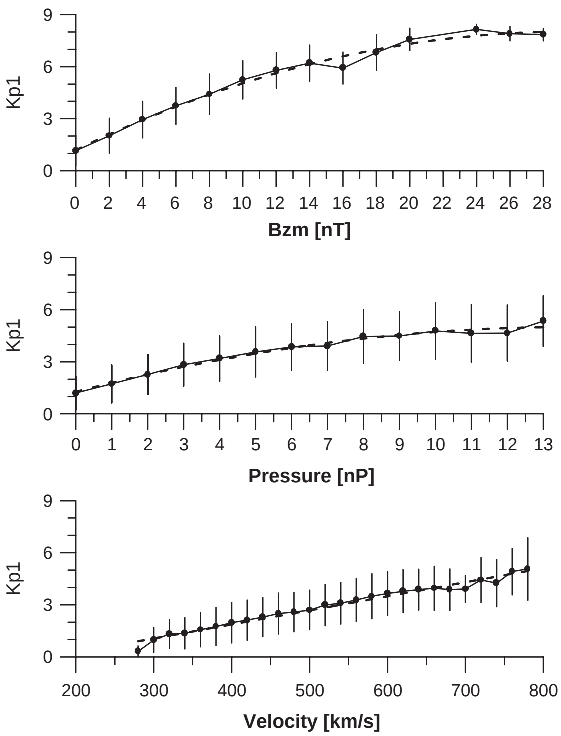

Fig. 4. Mean dependences of K_{p1} on B_{zm} (top), solar wind dynamic pressure (middle) and velocity (bottom). Dots show the mean values in the bins along X axis, vertical bar length represents $+/-$ standard deviation, while the dashed lines show the approximation of the mean values.

which obviously reflects in the cross-correlation. In this paper we do not attempt to resolve this relationship. We rather use the cross-correlation as a criterion of how significant the corresponding solar wind parameter to the model of K_{p1} is based on this figure, we conclude that the main dependence of K_{p1} should include, besides B_{zm}, solar wind velocity and dynamic pressure as well. Fig. 4 shows the mean dependence of K_{p1} on each of these solar wind parameters. The solid dots represent the mean values, obtained by averaging all available data within the corresponding bins, and are placed on the left border of each bin. The vertical bars represent the scatter of the data and their length is equal to twice the standard deviation of data around the mean. The dashed lines show the best approximations to the mean dependences: parabolic between K_{p1} and B_{zm} and between K_{p1} and the dynamic pressure, and linear with the ion velocity. We therefore consider the K_{p1} model in the form:

$$K_{p1} = a_0 + a_1 B_{zm} + a_2 P + a_3 V + a_4 B_{zm}^2 + a_5 P^2. \qquad (2)$$

As was mentioned above, the K_{p1} model of MA contained the dependence on B_{zm} only and the time constants T_1 and T_2 they calculated reflected that dependence. We expect that the new expression (2) will define different values of the time constants. Following the same approach as MA, we

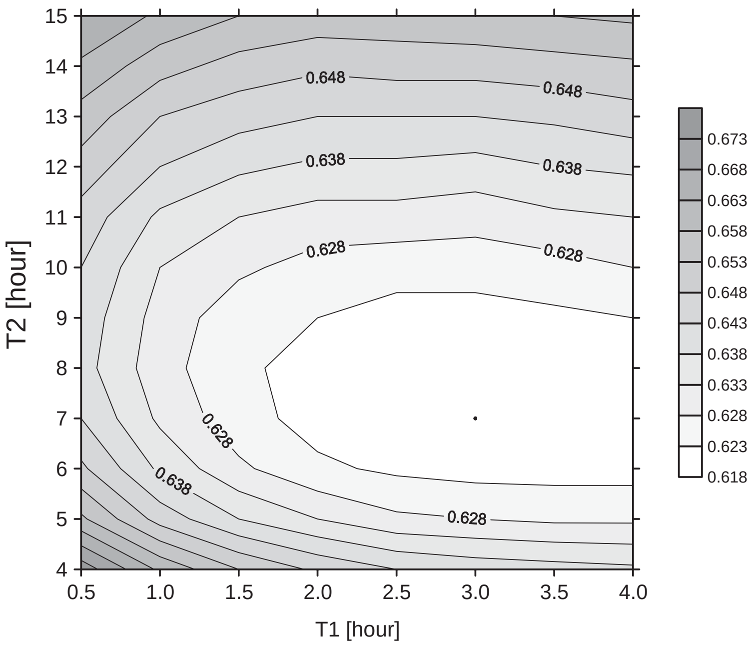

Fig. 5. Contours of constant model error, calculated by using variable values of time constants T_1 and T_2. It is assumed that the time constants $T_1 = 3$ and $T_2 = 6$ h, yielding the lowest model error, best represent the delayed reaction of B_{zm} to B_z changes.

now calculate K_{p1} fitting Eq. (2) to the values of B_z, P and V at each hour within the whole ACE database, compare it with the corresponding observed K_{p1} and calculate the model error as the root mean square deviation. Every fit uses a pair of time constants (T_1, T_2) and yields its own set of constants a_i and a model error. For a given hour, the fitting is repeated for a grid of pairs of T_1 (step 0.2 in the range 0.2–4.0 h) and T_2 (step 1.0 h in the range 4–24 h) which equals to $20 \times 20 = 400$ grid points. Model errors, obtained for each pair of time constants over the whole database, are accumulated and averaged. Fig. 5 shows a contour plot of the averaged model errors along T_1 and T_2 axes. Contours of constant error magnitudes are drawn with solid lines. We assume that the pair of time constants with the lowest model error best represents the delayed reaction of B_{zm} to B_z changes. Therefore, for further analysis we take $T_1 = 3.0$ h and $T_2 = 7.0$ h. With these time constants, the model expression for K_{p1} becomes:

$$K_{p1} = -2.3 + 0.64B_{zm} + 0.31P + 0.007V - 0.24B_{zm}^2 - 0.01P^2. \quad (3)$$

The coefficients a_i are obtained by fitting (2) to the whole database, with $T_1 = 3$ and $T_2 = 7$ h. Fig. 6 shows a comparison between K_{p1} observed during 1–19 August and 16–28 September 2000 and the corresponding model values. The thin line shows K_{p1} values and the solid line presents the model prediction. The agreement between the model and observations in these samples is acceptable. The model overestimates the peak values of K_{p1} during its sharp increase on 12 August and 18 September 2000. Both increasing and decreasing parts of K_{p1} changes, however, are well reproduced. The average root mean square deviation between the

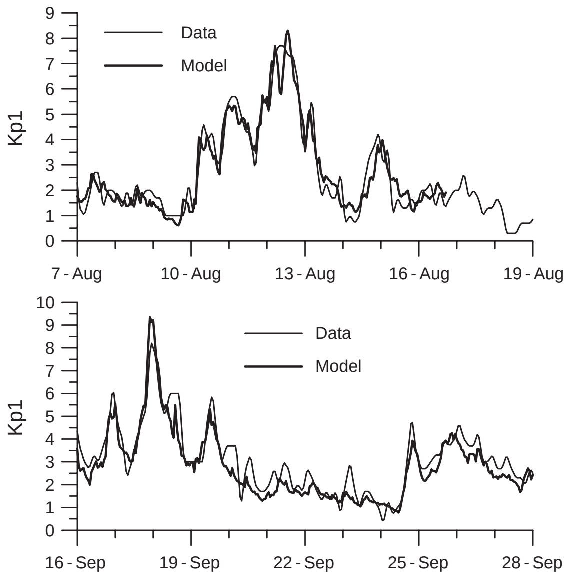

Fig. 6. Observed (thin line) and modelled (solid line) K_{p1} for the periods of 7–18 August 2000 (a) and 16–27 September 2000 (b).

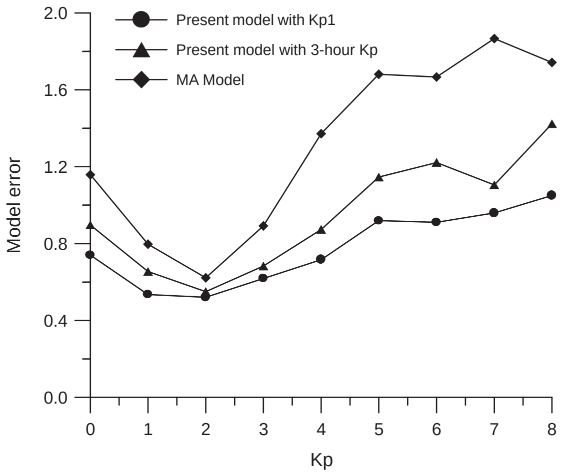

Fig. 7. Model error (diamonds) calculated for each a-unit-wide bin of the K_p magnitude.

observed and model K_{p1}, estimated over the whole database (overall model error) is 0.63 K_p units. Fig. 7 compares the model error of MA with that of the present model, calculated separately in a-unit-wide bins of K_p magnitude. The model error estimated from the 3-h K_p data set only is 0.72 K_p units, or about 14% higher than that estimated from the whole K_{p1} set. The difference obviously is due to the contribution of the interpolated K_{p1} values having lower standard deviation. The model error of MA is 0.96 K_p units. The minimum K_{p1} error of 0.52 is found around $K_p = 2$, which coincides with the most likely K_p value. At $K_p = 8$, the error increases to 1.05. Corresponding errors, when the model is applied to the 3-h K_p values only, are 0.55 and 1.7, respectively. The present model error is less than that of MA with 0.1 at $K_p = 2$ and with 0.9 at $K_p = 8$.

3. Discussions

Using the analogy with an electric circuit scheme, the so-called DRC circuit, MA obtained an analytical expression of the delayed reaction of K_{p1} to the faster changes of IMF B_z. The new quantity B_{zm} correlates much better with K_{p1} (reaching a maximum cross-correlation of 0.7) than B_z does (maximum of -0.4). In the present paper we improve the model by adding dependences on solar wind velocity and dynamic pressure, whose cross-correlations with K_{p1} are also significant. The mean dependences of K_{p1} on these three quantities determine how each of them enter the model expression: B_{zm} and P as parabolas and V as a linear function. The constants a_i are obtained by fitting expression (2) to the data from the whole available ACE database. The inclusion of additional terms to K_{p1} model requires obtaining of new values of the time constants T_1 and T_2 in the expression of B_{zm} (1). Fig. 5 shows that expression (3) with $T_1 = 3.0$ and $T_2 = 7.0$ h fits best to the data. These values differ from those obtained by MA ($T_1 = 0.8$ and $T_2 = 9$ h) using an expression on B_{zm} only. The new terms in linear regression (2) now capture some of the deviations between the data and B_{zm}, which in MA analysis have been assigned to the time delayed process. It is clear that the present approach cannot define a physically meaningful time delay between the force from solar wind parameters and K_{p1} reaction. This time delay will depend on the parameters included in the regression.

Della-Rose et al. (1999) have introduced "K-like" geomagnetic indices with variable time intervals (JD index), which were designed to represent geomagnetic activity with different time resolution. These authors found that the average value of their JD index strongly depends on the time window of averaging. At 1-h time-window the average JD value is about 30% less than the value averaged in the standard 3-h time window. Della-Rose et al. (1999) raised the question of how accurate is the standard 3-h K_p index in representing the geomagnetic activity within the time scales about an hour or less. In the present analysis we simplified the problem, formally increasing the number of K_p values. This hourly interpolation of the 3-hour K_p index is roughly equivalent to the averaging within a 3-h time window, sliding it with 1-h step. In the same way Della-Rose et al. (1999) have computed their 3-h index sliding it with 15-min step.

The overall model error, that is the mean root square deviation of model from the data, is estimated at 0.63 K_p units. The model error depends on K_p magnitude, having minimum value of 0.52 at $K_p = 2$ and increasing to 1.05 at $K_p = 8$. When the error is estimated only by the 3-h K_p values, with the moderate, interpolated values excluded, the error increases to 0.72, or with 14%. A rough comparison of this error with another sources of K_p prediction shows a marked advantage of the present approach. Boberg et al. (2000) have shown a model error of 0.60 at $K_p = 2$ and 2.80 at $K_p = 8$. Costello (1997) estimation showed values of 0.60 and 1.50, respectively. The model error obtained here improves the accuracy achieved by MA by 30%.

4. Conclusions

A new model relating K_p to the solar wind parameters is developed, using the analogy with a time-delayed output voltage in a DRC electric circuit. The model includes the previously defined B_{zm} function, solar wind velocity and dynamic pressure. These quantities show the highest correlation with K_p. To enlarge the statistics, the model is derived by using the hourly interpolated K_p values, denoted here as K_{p1}. The regression fit with the data from 3 years of ACE measurements shows that the average root mean square deviation between the model and observations (model error) is 0.63. The model error decreases with 14% when the 3-h K_p values only are used for testing. The accuracy of the present model compared with the previous MA model is increased with about 30%. It is found higher than the accuracy of the models currently forecasting K_p.

References

Baker, D., Klimas, A., McPherron, R., Buchner, J., 1990. The evolution from weak to strong geomagnetic: an interpretation in terms of deterministic chaos. Geophysical Research Letters 17 (1), 41–44.

Boberg, F., Wintoft, P., Lundstedt, H., 2000. Real K_p predictions from solar wind data using neural networks. Physics Chemistry Earth 25 (4), 275–280.

Costello, K.A., 1997. Moving the Rice MSFM into a real-time forecast mode using solar wind driven forecast models. Ph.D. Dissertation, Rice University, Houston, TX, June 1997.

Della-Rose, D.J., Sojka, J.J., Zhu, L., 1999. Resolving geomagnetic disturbances using "K-like" geomagnetic indices with variable time intervals. Journal of Atmospheric and Solar-Terrestrial Physics 61, 1179–1194.

Hones Jr., E., 1979. Transient phenomena in the magnetotail and their relation to substorms. Space Sciences Review 23, 393–412.

Kamide, Y., Baumjohann, W., Daglis, I., Gonzalez, W., Grande, M., Joselyn, J., McPherron, R., Phillips, J., Reeves, E., Rostoker, G., Sharma, A., Singer, H., Tsurutani, B., Vasyliunas, V., 1998. Current understanding of magnetic storms: storm–substorm relationships. Journal of Geophysical Research 103 (8), 17705–17728.

Klimas, A., Baker, D., Roberts, D., 1991. Linear prediction filters for linear and nonlinear modeled geomagnetic activity. Geophysical Research Letters 18 (8), 1635–1638.

Klimas, A., Baker, D., Roberts, D., Fairfield, D., Buchner, J., 1992. A nonlinear dynamic analogue model of geomagnetic activity. Journal of Geophysical Research 97 (A8), 12253–12266.

Muhtarov, P., Andonov, B., 2000. Improved relationship between the IMF component B_z and K_p index. Bulgarian Geophysical Journal 26 (1–4), 165–172.

Vassilliadis, D., Sharma, A., Papadopoulos, K., 1993. An empirical model relating the auroral geomagnetic activity to the interplanetary magnetic field. Geophysical Research Letters 20 (16), 1731–1734.